Supporting Information: Surface states on photonic crystals as hybrid dielectric metasurface bound states of the termination layer

Anna C. Tasolamprou,[*,†] Lei Zhang,[‡] Eleftherios N. Economou,[†,¶] Costas M. Soukoulis,[†,‡] and Thomas Koschny[‡]

†*Institute of Electronic Structure and Laser, Foundation for Research and Technology Hellas, N. Plastira 100, 70013 Heraklion, Crete, Greece*

‡*Ames Laboratory and Department of Physics and Astronomy, Iowa State University, Ames, Iowa 50011, USA*

¶*Department of Physics, University of Crete, Heraklion, Greece*

E-mail: atasolam@iesl.forth.gr

In the Supporting Information we discuss additional theoretical details for the hybrid surface states dispersion, including the 3D analog, and additional information concerning the experimental investigation. The document includes, 11 pages, 7 figures and 3 sections:

S1. Additional details for the hybrid surface states dispersion in corrugated photonic crystals.

S2. Experimental setup and additional results from simulation and experimental measurements for the finite corrugated photonic crystal.

S3. Hybrid surface states dispersion in corrugated three dimensional photonic crystals.

S1 Additional details for the hybrid surface states dispersion in corrugated photonic crystals

In this section we present additional detailed numerical results for the corrugated photonic crystal focusing i) on the effect of the variable size of the rods in the termination corrugated layer and ii) on the effect of its separation distance from the bulk photonic crystal with respect to variable wavevector k.

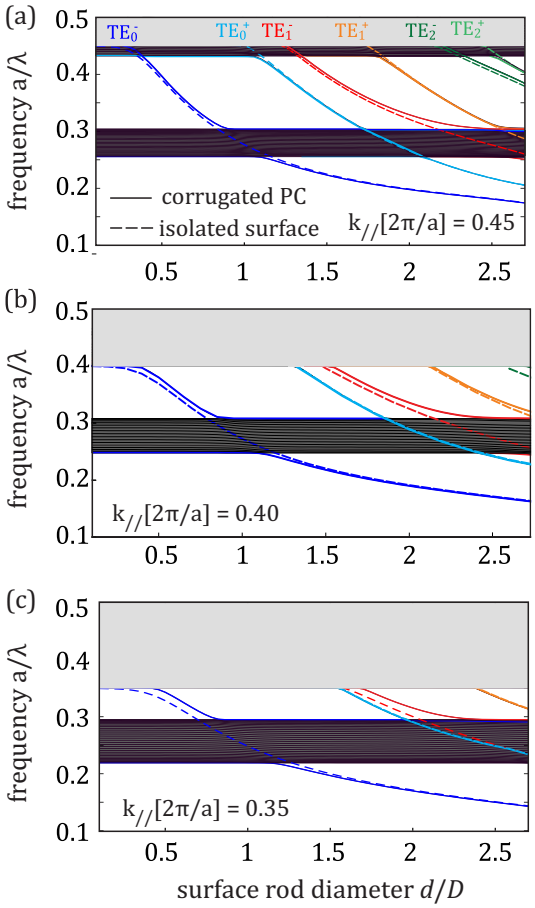

Figure S1: Dispersion diagram of the TE_0^-, TE_0^+, TE_1^-, TE_1^+ and TE_2^-, TE_2^+ surface modes in the combined system of photonic crystal (solid lines) and the isolated metasurface row (dashed lines) with respect to the row rod size d normalized over the photonic crystal rod size D for (a) $k = 0.45$, (b) $k = 0.40$ and (c) $k = 0.35$.

Figure S1 presents the dispersion diagram of the supported bound states in the combined system of the bulk photonic crystal and the corrugated surface (shown in solid lines) and

the isolated metasurface (shown in dashed lines) when the size of the termination corrugated rods, d, varies in the range $d/D = [0.3 - 2.7]$, where D is the size of the rods of the bulk photonic crystal. In particular we plot the fundamental mode TE_0^- (shown in blue) and the higher modes TE_0^+, TE_1^-, TE_1^+ and TE_2^-, TE_2^+. The dispersion is calculated at fixed wavevector values, k, $k = 0.45$ in Figure S1(a), $k = 0.40$ in Figure S1(b), and $k = 0.35$ in Figure S1(c). We observe that the bound modes of the system remain intact in the bandgap of the photonic crystal, below the light line and very close to the dispersion of the isolated metasurface for all d values, besides around the $d/D = 1$ regime. Around $d/D = 1$, the fundamental bound mode, TE_0^-, as well as the higher TE_1^- and TE_2^- bound modes hybridize with the dielectric band of the bulk photonic crystal while remaining unaffected by the air band of the photonic crystal due to the spatial profile (mis)match as explained in the main manuscript. Due to the spatial profile (mis)match, TE_0^+, TE_1^+ and TE_2^+ bound modes hybridize with the air band and not with the dielectric band of the bulk photonic crystal. Moreover as seen in Figure S1, for lower k values the deflection of the surface states in the presence of the photonic crystal bands is higher.

In Figure S2 we present the numerically calculated dispersion of the fundamental TE_0^- bound mode with respect to the separation distance between the bulk photonic crystal and the surface corrugation, L/a. We investigate cases of variable d/D values, assuming a fixed wavevector value, in particular, $k = 0.45$ shown in Figure S2(a), $k = 0.40$ shown in Figure S2(b), and $k = 0.35$ shown in Figure S2(c). We observe that when the corrugation is close to the bulk photonic crystal the impact in the dark state eigenfrequency is significant. In contrast, with increasing separation distance, the combined system's bound mode saturates to the isolated surface bound mode eigenfrequency, which marked with the dots in the right vertical axis in Figures S2(a-c). Once again we observe that the $d/D = 1$ state hybridizes with the dielectric bulk modes of the crystal and that the $d/D = 0.4$ bound state coexist in frequency (but not in space) with the air band bulk photonic crystal modes. It is interesting to see additionally, that in the case of $L/a < 1$ even the d/D corrugation provides a surface

mode as it merges with the last row of the bulk photonic crystal.

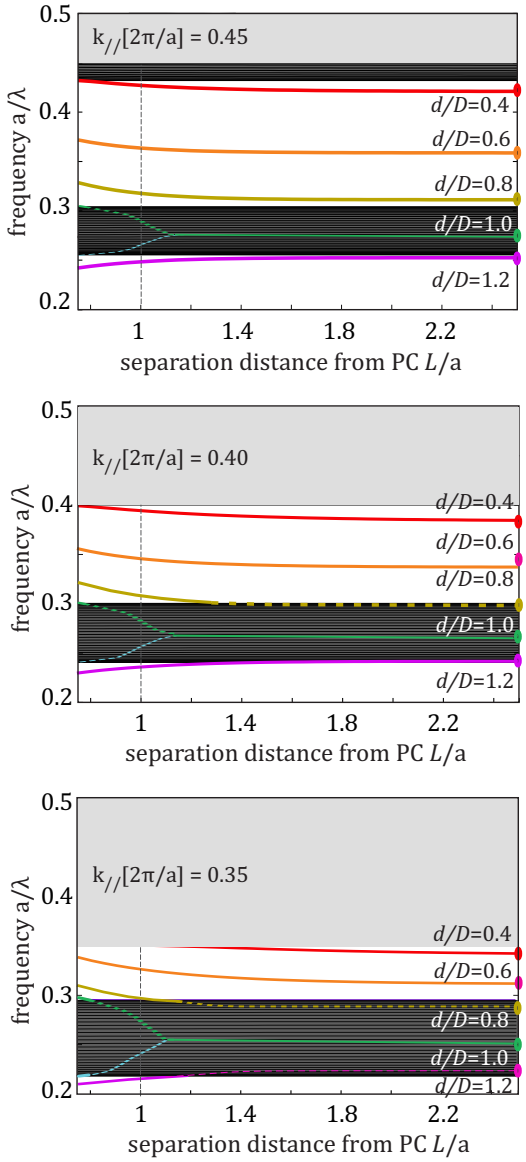

Figure S2: The dispersion of the TE_0^- surface mode in the combined system with respect to the separation distance of the corrugated metasurface form the photonic crystal for various d/D values and fixed wavevector (a) $k = 0.45$, (b) $k = 0.40$, (b) and $k = 0.35$. Distance $L/a = 1$ corresponds to the lattice of the crystal and it is marked with the dashed line.

S2 Experimental setup and additional results from simulation and experimental measurements for the finite corrugated photonic crystal

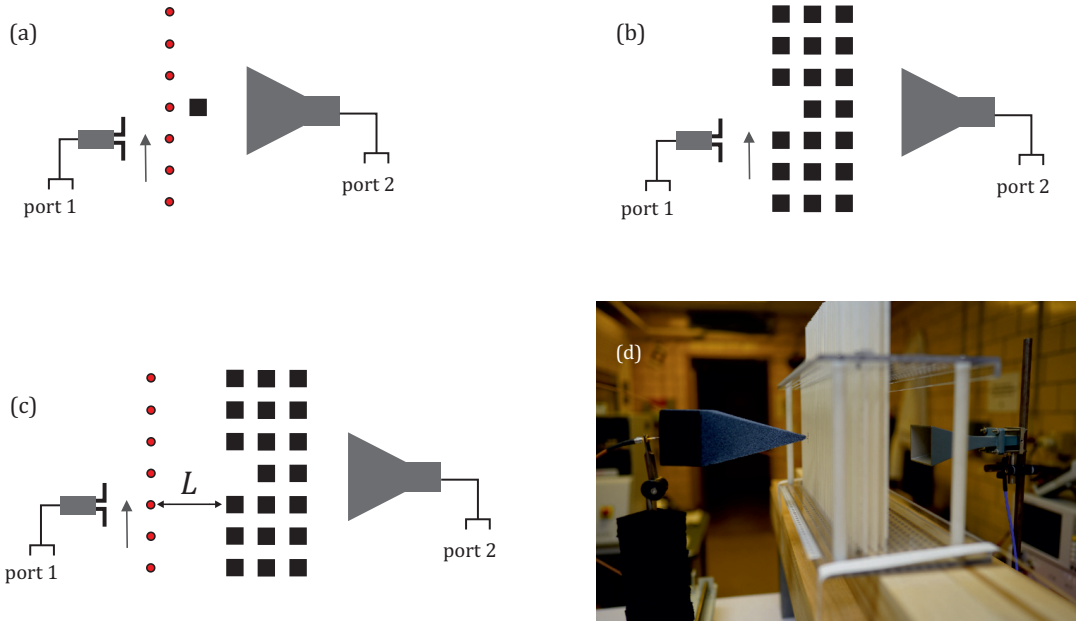

Figure S3: (a)-(c) Schematic of the setups and the structures for the experimental characterization of the surface states in the hybrid structures, referring to the characterization of the isolated metasurface and the corresponding corrugated photonic crystal. The surface modes are excited by a broad beam coming from a horn antenna incident on the far side of (a) an isolated metasurface and couple via an additional scatterer, (b) the bare photonic crystal and (c) the combined system of the corrugated photonic crystal and couple via a void scatterer (single missing rod) in the center of the last row of dielectric rods of the bulk photonic crystal. (d) Image of the experimental set up taken during the characterization at Ames Laboratory.

For the experimental characterization we use photonic crystal structures of a finite square lattice with a lattice constant of 11 mm made of square alumina rods ($\varepsilon = 9.8$) with a cross-section of 3.15 mm^2 that is terminated on one side by a corrugation layer of thinner circular rods of the same material with a diameter of 1.83 mm. The truncated photonic crystal has 6 layers of 38 rods each, followed by the corrugation layer in the next lattice position. The structure is illuminated by a broad, approximately Gaussian beam in the range 8-13

GHz, from the side distal to the corrugation layer, while the field profile of the surface mode is observed by scanning a small, sub-resonant dipole antenna along a line parallel to the surface 2 mm in front of the corrugation layer as function of frequency using an automated 2D positioning stage. The complex scattering amplitudes of the near field are measured using an Agilent E8364B network analyzer. The schematic and the image of the setup are shown in Figure S3.

S2.1 *Isolated metasurface*

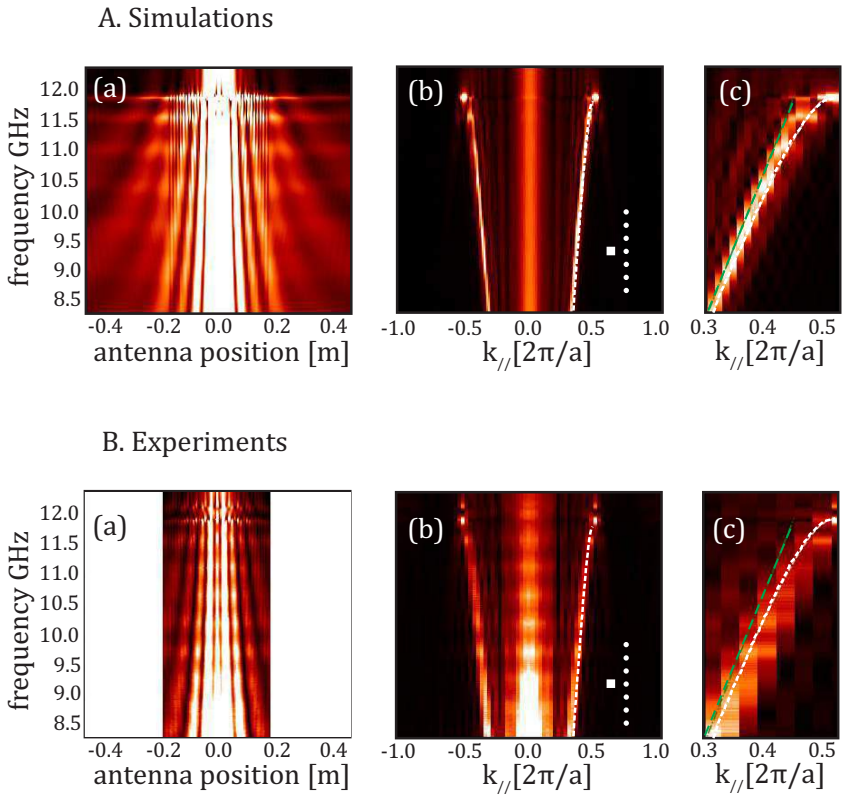

Figure S4: A. Simulation and B. experimental measurement tracing the bound modes sustained in the isolated metasurface. The bound modes are excited by a broad Gaussian beam incident on the far side of the metasurface and couple via a scatterer. A/B(a) show the spatial intensity distribution along the metasurface as function of frequency, A/B(b) show the bound state dispersion diagram calculated with the Fourier transform of A/B(a). A/B(c) show a magnified view of the bound mode brach; the dashed white lines indicate the bound mode dispersion for the isolated infinite metasurface. The green dashed line shows the light line in air.

We initially study the dispersion properties of the isolated metasurface consisting of the thinner circular rods with a diameter of 1.83 mm as shown in Figure S3(a). To excite the bound mode of the system, we use an incident Gaussian beam coming from the horn antenna which is placed on the far side of the metasurface. To couple the horn antenna free-space radiation to the bound mode, we use an additional scatterer in the form of a missing rod. This is shown in Figure S3. The distribution of the near field is assessed by measuring the complex amplitude of the field at a position 2 mm in front of the metasurface. The distribution of the near field with respect to the frequency is calculated and experimentally measured in Figure S4A(a) and Figure S4B(a), respectively. To assess the dispersion, we employ a spatial Fourier transform in the near field data and we present the results in Figure S4A/B(b). A detail view of the dispersion in Figure S4A/B(c) reveals how the branch of the bound mode lights up in the dispersion diagram and how it follows the infinite metasurface's dispersion shown with the dashed white lines in Figure S4A/B(c). The green dashed line shows the light line in air for comparison.

S2.2 *Corrugated photonic crystal*

In this section we provide additional/intermediate results used for the experimental investigation of the corrugated photonic crystal presented in the main text.

In Figure S5 we present cross-section plots along the frequency axis for the five experimentally measured surface separations for both, simulations and measurements, i.e., 10 mm, 11 mm, 12 mm, 22 mm, and 33 mm. In order to discriminate noise and obtain the clearest possible identification of the surface mode peaks, the power density at the position of the antenna (2mm in front of the corrugated surface) integrated spatially along the surface has been shown with respect to the frequency. The orange circles indicate the fitted peak positions. Note that in contrast to the rather clean simulation data, the measurements contain significant noise, mostly originating from multiple reflections inside the antenna cables (nearly periodic oscillations with a period of around 500 MHz) and from stray free-space

reflections in the lab.

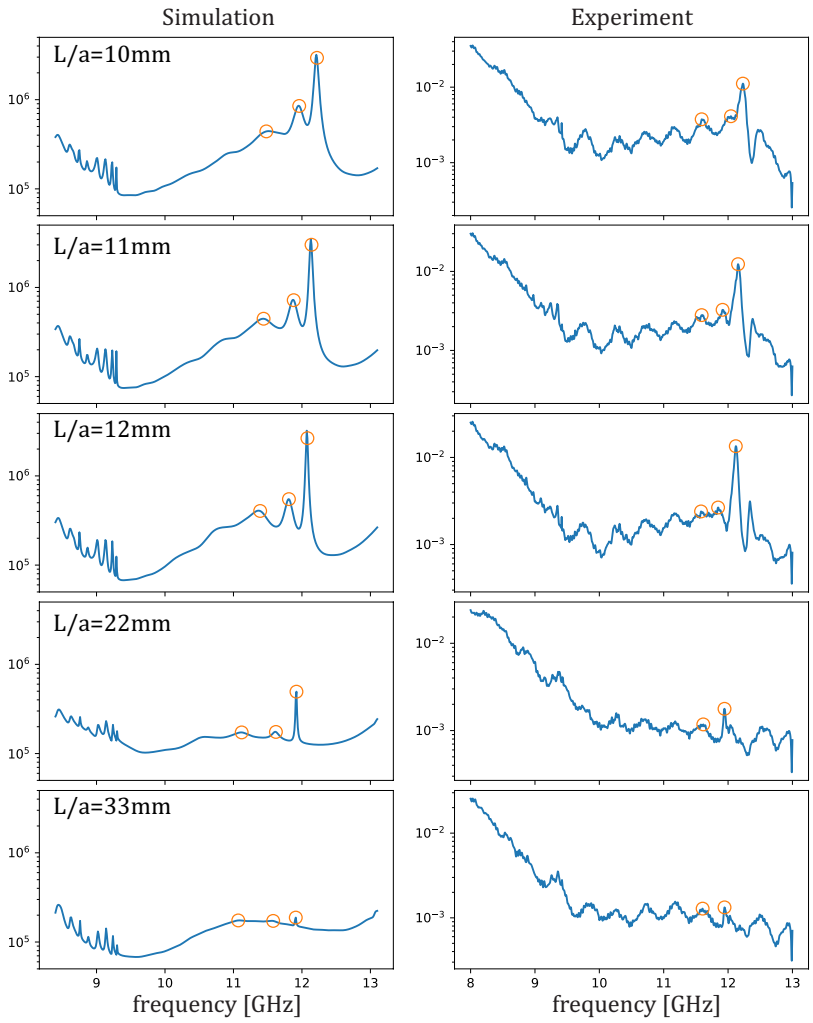

Figure S5: Frequency cross-sections: The Peak positions to identify first few discrete surface modes for the corrugated PC are shown, corresponding to the five cases of surface separations that were used in the experiment: 10 mm, 11 mm (a), 12 mm, 22 mm (2a), and 33 mm (3a). To discriminate noise, instead of the frequency cross-section at a fixed antenna position, the power density integrated along the surface is plotted vs. frequency. The left column show the peaks for the numerical simulations, the right column the corresponding peaks as observed in the experiment. The orange circles indicated the identified surface mode locations that were used to produce the traces in Figure 6 in the main manuscript.

In Figure S6 we present the numerical simulations showing the field distributions as magnitude (left) and real part (right) of the simulated electric filed distributions E_z (i.e., the component perpendicular to the image plane) of the first three surface modes at 12.08, 11.81, and 11.39 GHz are shown for the finite, corrugated PC with a square lattice (a=11mm)

assuming that the separation of the corrugation layer is 10mm. We observe the strong excitation of the surface mode, as predicted by the theory.

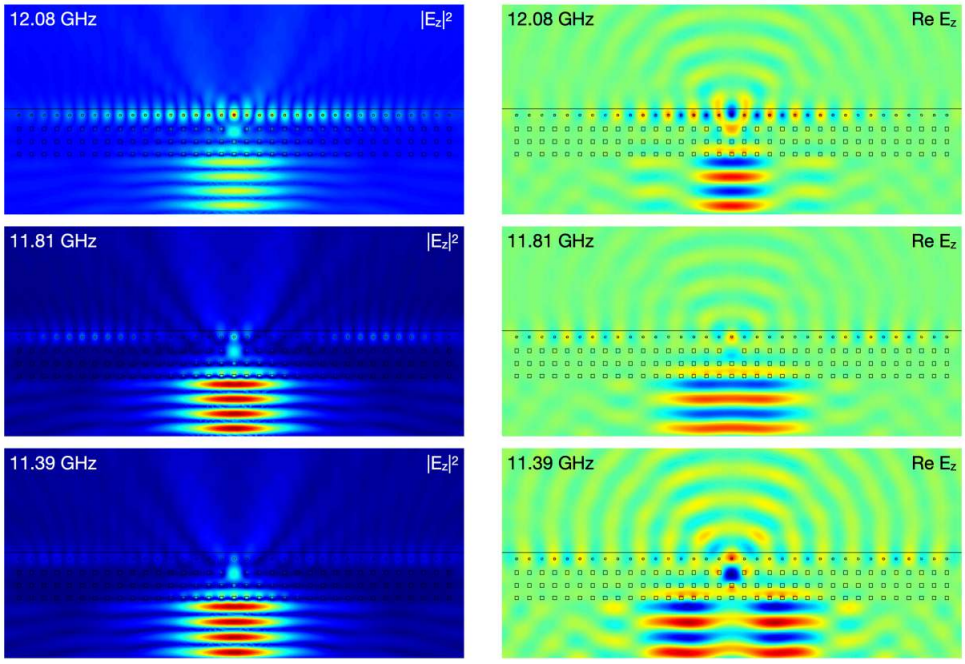

Figure S6: The field distributions as magnitude (left) and real part (right) of the simulated electric field distributions E_z (i.e., the component perpendicular to the image plane) of the first three surface modes at 12.08, 11.81, and 11.39 GHz are shown for the finite, corrugated PC with a square lattice (a=11mm). The separation of the corrugation layer is 10mm. Excitation is from the bottom of the figure with an approximately Gaussian beam. The simulation geometry and parameters correspond to the experimentally measured finite, corrugated PC. A comparison of the simulated and experimentally measured surface modes is shown in Figure 6 of the main paper.

S3 Hybrid surface states dispersion in corrugated three dimensional photonic crystals

In this section we present a theoretical demonstration of the hybrid surface states for a corrugated 3D photonic crystal. We assume a three dimensional photonic crystal of dielectric rectangular bricks with dimensions d_x, d_y, d_z, placed in a cubic lattice formation, $a = a_z = a_y = a_z = 11$ mm. We also assume a three dimensional crystal made of rectangular bricks

with dimensions, D_x, D_y, D_z placed in the same cubic lattice formation, $a = a_z = a_y = a_z =$ 11 mm. As proof of concept we assume only the case where the metasurface lies on top of the bulk 3D photonic crystal at a distance equal to the lattice, $L = a$, and investigate the case of variable d_x/D_x, with $D_x = 5$ mm, while $d_y/D_y = 8$ mm and $d_z/D_z = 6$ mm. The permitivity of the rods is $\varepsilon = 9.8$ and they stand in air.

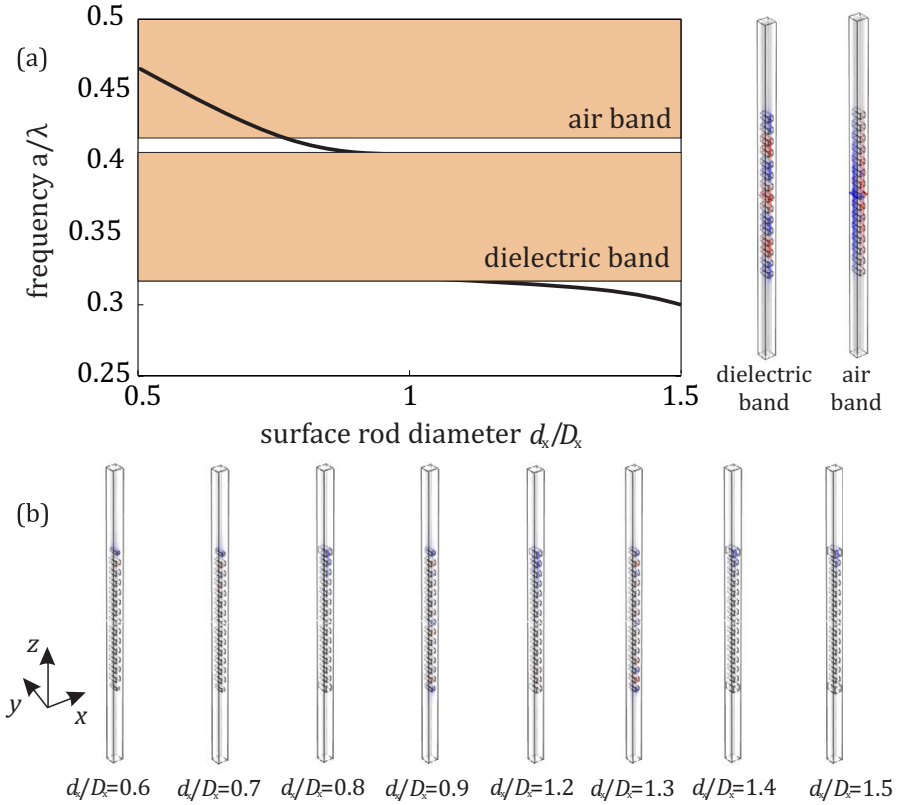

Figure S7: Fundamental surface modes on a corrugated 3D photonic crystal for varying size of the dielectric bricks of the corrugation layer versus the bulk 3D photonic crystal. The 3D photonic crystal consists of a cubic lattice of discrete bricks with dimensions D_x, D_y, D_z. A slab of bulk photonic crystal is terminated by a corrugation layer of similar bricks but with dimensions d_x, $d_y = D_y$, $d_z = D_z$. (a) The band structure of the 3D corrugated system which clearly shows a surface mode, which, in analogy to the 2D case discussed in the main manuscript, crosses the air band of the bulk photonic slab and disappears by hybridizing and merging onto the bulk states (dielectric band) of the bulk photonic slab for the case of vanishing corrugation (surface identical to bulk, $d_x/D_x = 1$). The field distributions of the dielectric and the air band are shown as an inset in (a). (b) Field distributions of the surface modes are shown for different size ratios, d_x/D_x, demonstrating the hybridizing and merging of the surface state onto the bulk photonic crystal modes.

In analogy to the to the 2D case discussed in the main manuscript, we investigate the

dispersion properties of the fundamental surface states in the 3D crystal assuming variable corrugation size, for simplicity only along the surface propagation direction x, d_x/D_x, i.e., we apply the same investigation as Figure 3 of the main text. We assume that the termination brick dimension d_x/D_x varies in the range [0.5-1.5]. Figure S7(a) shows the dispersion diagram of the fundamental surface mode in the corrugated crystal. The distribution of the electric field (real part) of the bulk modes in the supercell, dielectric band and air band, are shown in the left side of Figure S7(a), while the distribution of the electric field (real part) of the surface modes in the corrugated supercell are shown in Figure S7(b). As in the 2D case, we observe that the surface states dispersion crosses the high frequency air band and disappears by hybridizing and merging onto the bulk states (dielectric band) of the bulk photonic slab for the case of vanishing corrugation (surface identical to bulk, $[d_x/D_x = 1)]$, due to the spatial mis(match) between the corrugated surface modes and the uncorrugated bulk modes.